Astron. Astrophys. 259, 614–626 (1992)

ASTRONOMY AND ASTROPHYSICS

Dust model containing polycyclic aromatic hydrocarbons in various environments

R. Siebenmorgen and E. Krügel

Max-Planck-Institut für Radioastronomie, Auf dem Hügel 69, D/W-5300 Bonn 1, Germany

Received August 13, accepted December 14, 1991

Abstract. We analyze the IR spectra and the extinction curve in four kinds of astronomical environments: the solar neighborhood, two reflection nebulae (N 2023 and N 7023), a planetary nebula (N 7027) and an H II region (M42 = Orion A). The observations, including the high-resolution data of the IR features from polycyclic aromatic hydrocarbons (PAHs), are fit by a dust model that consists of three components: (i) Big grains with radii $a > 100$ Å of silicate and carbon. They are responsible for the far IR emission and the linear rise in the extinction curve. (ii) Small graphite particles (4 Å $< a \leqq 100$ Å) to explain the mid-IR emission and the 2175 Å extinction bump; (iii) PAHs which produce the near and mid-IR bands, part of the underlying continuum and the non-linear rise in the far-UV. We outline the method for calculating the radiation emitted by the particles including effects of quantum heating. The radiation field differs strongly in hardness and strength in the four types of selected sources and in Orion observations refer to different distances from the exciting star. Therefore, we can quantitatively assess the influence of the environment on the structure and abundance of the PAHs.

Key words: dust, extinction – infrared: interstellar: lines

1. Introduction

Interstellar dust has the remarkable property to absorb the stellar light and reemit it at infrared wavelengths. Because of its large abundance in many sources most of the energy is contained in the far IR. This is one of the strongest reasons why we have to search for a viable dust model.

Three kinds of observations coercively led to a modification of the classical dust concept, which was in use until the early eighties. They concern (a) the high flux ratios S_{12}/S_{100} and S_{25}/S_{100} in interstellar clouds as observed by IRAS (Boulanger & Perault 1988); (b) the near and mid-IR resonances seen in emission in very diverse sources; (c) the extremely high color temperatures (> 1000 K) in reflection nebulae independent of distance from the exciting star (Sellgren et al. 1985). All these observations cannot be explained by the classical dust model. Instead, they led to the now widely accepted idea that an additional component of very small dust particles is present in the interstellar medium. Their tiny size and consequently low heat capacity produces temperature fluctuations which result in color temperatures much higher than the time averaged temperature of the grain material. In addition, planar ensembles of a few aromatic carbon cycles, so called PAHs, seem to explain the observed IR features.

This paper has the goal to present a dust model that includes these very small particles and PAHs. We derive it by calculating the extinction and IR emission in selected sources where extinction measurements and high resolution spectral observations indicative of PAHs are available. In particular, we apply it to the solar vicinity, two reflection nebulae (NGC 2023 and NGC 7023), one planetary nebula (NGC 7027) and an H II region (ionization front in Orion A).

Send offprint requests to: R. Siebenmorgen

2. The dust model

The properties of interstellar grains are derived from (a) the constraints on cosmic abundance to the dust forming elements; (b) the interstellar extinction curve; (c) the resonances at 9.7 and 18 μm (attributed to silicates); (d) the broadband IR emission from heated dust as observed, for example, in star forming regions; (e) the narrow IR emission features (attributed to PAHs); (f) the wavelengths dependence and strength of polarization; (g) observations of scattered light; (h) IR absorption bands attributed to "ice"-mantles around grains shielded from UV radiation.

A review on those dust properties, which are today generally accepted, is given by Mathis (1990). Further information on particles is gained from laboratory studies (Bussoletti et al. 1988), especially with respect to their optical properties and surface reactions. In the following we discuss the major points of our model.

2.1. *The extinction curve and dust components*

The shape of the extinction curve depends on the environment of the grains. However, its various forms can be described by just one parameter, for which one may choose, for instance, $R = A_V/E_{B-V}$ (Cardelli et al. 1989). $R = 3.1$ corresponds to the diffuse interstellar medium, higher values to molecular clouds. The curve is tabulated by Mathis (1990). It can be divided into three wavelength regions (Fitzpatrick & Massa 1988), and in each region one particular ensemble of grains is responsible for the extinction.

2.1.1. The linear rise at $\lambda^{-1} < 2\,\mu m^{-1}$ and the big particles

As already shown by Mathis et al. (1977, MRN) this part of the extinction curve can be explained by particles, which we shall call big, with radii a between approximately 100 to 2500 Å. They are distributed in size according to $n(a) \propto a^{-3.5}$. The lower boundary is not well determined because one enters the Rayleigh limit and the upper boundary because of increasingly gray extinction. We calculate absorption and scattering efficiencies from Mie theory for compact spheres. In principle, more complex situations like grain mantles or a fluffy structure of the material could also be considered in various ways of approximation.

There are two kinds of big particles. First, "astronomical silicates" which produce the well known Si-O stretching and bending modes at 9.7 and 18 μm. For them we assume optical constants after Draine (1985) and a volume of $3.1\ 10^{-27}\,cm^3$ per hydrogen atom. This implies that all silicon with a cosmic abundance $Y_{Si} = 3.1\ 10^{-5}$ is locked up in grains and that the silicate material has a density $\varrho_{Si} = 2.5\,g\,cm^{-3}$. The second kind of large particles, distributed in size as the silicates, is made up of carbon. The carbon must be amorphous because it is not possible to explain the constancy of the central wavelength and the observed half-width in the 2175 Å bump with large graphites (Draine 1989). Optical constants for amorphous carbon are quite uncertain (e.g. Edoh 1983; Mathis & Whiffen 1989), but they can yield a very good approximation to the extinction curve (especially around 2500 Å). Nevertheless, because of their widespread use we again employ optical constants from Draine (1985), although they refer to graphite. Per hydrogen atom we assume a volume of $2.1\ 10^{-27}\,cm^3$ of carbonaceous material in big grains. This corresponds to a bulk density $\varrho_C = 2.3\,g\,cm^{-3}$ and a carbon abundance in these grains of $Y_c = 2.4\ 10^{-4}$. The rest of the carbon abundance in solids of $6\ 10^{-5}$ is assumed to reside in the small graphite grains and in PAHs.

2.1.2. The resonance at 2175 Å and small graphites

The shape of this resonance can be approximated by a Drude-profile and shows very little variation of the central wavelength λ_c (for two thirds of the observed stars $\lambda_c = 2175 \pm 10$ Å), but a scatter for the half-width of $\gamma = 0.992 \pm 0.12\,\mu m^{-1}$ (Fitzpatrick & Massa 1988). The best candidate for explaining the bump are small graphite particles (Draine 1989; Sorrel 1990). They have a strong resonance around 2200 Å which becomes size-independent in the Rayleigh-limit ($2\pi a \ll \lambda$), i.e. when $a \leqq 70$ Å. The variations in γ may be due to changes in the surface, rather than the size (Draine 1988). To produce the resonance with graphite the relative abundance of the carbon atoms with respect to hydrogen must be $Y_C^{gr} \approx 5\ 10^{-5}$. Very small graphite grains ($a < 20$ Å) become unstable (Nuth 1987). An absolute lower limit to the grain radius follows from the sublimation rate and lies around 5 Å (Guhathakurta & Draine 1989). We use graphites with a size distribution $n(a) \propto a^{-4}$ with $a \in [4, 100]$ Å (Draine & Anderson 1985) and $\varrho_C = 2.3\,g\,cm^{-3}$.

Mie theory becomes inaccurate for very small grains and the measurement of optical constants is uncertain in view of surface effects, irregular shape and impurities (Huffmann 1989). We use for the absorption efficiency Q in the 2175 Å resonance for $\lambda < 0.5\,\mu m$ a Drude-profile

$$\frac{Q}{a} = c_1\,x + \frac{c_2\,x^2}{(x - x_0)^2 + \gamma^2\,x^2}\ [cm^{-1}] \qquad (2.1)$$

with $c_1 = 6.6\ 10^4$, $c_2 = 1.92\ 10^6$ and wavenumber $x_0 = \lambda_c^{-1}$, x in cm^{-1} and for $\lambda > 0.5\,\mu m$ we use Mie theory with optical constants from Draine (1985).

For calculating the emission spectrum of these small particles one has to take into account their temperature fluctuations. This requires knowledge of the specific heat or enthalpy $U(T)$. An analytic approximation to $U(T)$ of graphite in erg/atom is given by Chase et al. (1985):

$$U(T) = \frac{4.15\ 10^{-22}\,T^{3.3}}{1 + 6.51\ 10^{-3}\,T + 1.5\ 10^{-6}\,T^2 + 8.3\ 10^{-7}\,T^{2.3}} \qquad (2.2)$$

One has to consider the decoupling of translational and rotational from the vibrational degrees of freedom. This leads to a correction factor for $U(T)$ (Guhathakurta & Draine 1989) of $(1 - 2/N)$, where N is the number of atoms in the grain. So this correction has only to be considered for the smallest particles.

2.1.3. The non-linear rise in the FUV and the PAHs

There are basically three explanations to the increase of the extinction curve at $\lambda^{-1} > 5.9\,\mu m^{-1}$. (a) The FUV rise is at the wing of a second graphite resonance at 700 Å; (b) Small silicate grains (Sorrel 1989); (c) PAHs (Leger et al. 1989a). We favor the latter explanation. Laboratory measurements in the optical and UV and FUV of various PAHs (benzene, naphtalene, coronene) have shown that they possess strong absorption cross sections due to electronic transitions ($\pi \rightarrow \pi^*$, $\pi \rightarrow \sigma^*$). Their spectra in the visual and UV are dominated by strong bands around 2000 to 2500 Å and a series of almost continuous weak bands which increase in strength from 2000 to 1000 Å (Robin 1974). A mixture of such particles shows a non-linear increase in the far UV as it is observed in the extinction curve. A summary on the PAH properties used in our model follows below.

2.2. Polycyclic aromatic hydrocarbons (PAHs)

Starting with Gillett et al. (1973) one observed between 3 and 14 μm a family of resonances in very diverse sources such as reflection and planetary nebulae, H II regions and even extragalactic objects. We follow Léger & Puget (1984) and Allamandola (1985) who proposed large isolated molecules (PAHs) to explain the near and mid IR emission features. With increased spectral resolution also less pronounced resonances could be detected (de Muizon et al. 1986; Allamandola et al. 1989).

2.2.1. Spectral features

We calculate the emission from the five strongest IR resonances at 3.3, 6.2, 7.7, 8.6 and 11.3 μm as well as from the underlying continuum. The wavelength range from 2.5 to 5 μm is dominated by the fundamental transition ($v = 1 \rightarrow 0$) at 3.29 μm characteristic for C–H aromatic stretching. We neglect other observed weaker features, such as the aromatic C–H stretch at 3.4 μm ($v = 2 \rightarrow 1$). The 6.2 and 7.7 μm resonance refer to aromatic C=C stretching and the one at 8.6 μm is due to C–H in-plane bending. The profiles and center positions of the 7.7 μm feature vary among sources.

The region between 10 to 20 μm is dominated by a resonance between 10.5 to 13.5 μm due to C–H out-of-plane aromatic bending. It generally has its center at 11.3 μm, but sometimes it is shifted to longer wavelengths depending on the number of peripheral H-atoms in the edge carbon rings. The line center at 11.3 μm is due to a mono C–H vibration. From the pre-

ponderence of λ_c around 11.3 μm one concludes that the edge rings contain only isolated, non-adjacent peripheral hydrogen atoms. This constrains the geometry of the PAHs. Furthermore, PAHs with many peripheral H bonds are less stable and therefore less frequent. Between 20 to 100 μm the resonances are characteristic for individual PAH molecules. The bands vary strongly in position and form and are explained as C−C−C vibrations. High vibrational excitation of the molecules produces a quasi-continuum due to overlapping of many weak bands in the near and mid IR.

2.2.2. Absorption cross sections

We denote by σ^{big}, and σ^{gr} and σ^{PAH} the cross section per hydrogen atom of the big grains, the small graphites and the PAHs. We assume that the absorption cross section of a PAH is proportional to the number of its carbon atoms. Because the total extinction cross section $\sigma^{tot}(\lambda) = \sigma^{big}(\lambda) + \sigma^{gr}(\lambda) + \sigma^{PAH}(\lambda)$, $\sigma^{PAH}(\lambda)$ follows from

$$\sigma^{PAH}(\lambda) = \frac{\sigma^{tot}(\lambda)}{\sigma^{tot}(V)} \{\sigma^{big}(V) + \sigma^{gr}(V) + \sigma^{PAH}(V)\} - \sigma^{big}(\lambda) - \sigma^{gr}(\lambda) \quad (2.3)$$

where the ratio $\sigma^{tot}(\lambda)/\sigma^{tot}(V)$ is given by the extinction curve. For the purpose of calculating $\sigma^{PAH}(\lambda)$ one may neglect $\sigma^{PAH}(V)$ because it is small compared to the two other terms in the bracket. However, it can be estimated after Desert et al. (1990)

$$\sigma^{PAH}(V) = 1.7\ 10^{-18}\ Y_C^{PAH}\ [\mathrm{cm^2/H\ atom}] \quad (2.4)$$

where Y_C^{PAH} is the fraction of carbon atoms per H atom locked up in PAHs (see Sect. 2.2.3). Dividing Eq. (2.3) by Y_C^{PAH} gives the absorption cross section of a PAH per C atom. With $Y_C^{PAH} \simeq 3\ 10^{-5}$ one obtains rough agreement with laboratory measurements (Leger et al. 1989a).

2.2.3. Abundance of PAHs

We first derive an overall estimate. The mean extinction in the visual is $\kappa_V = 4.6\ 10^{-22}\,\mathrm{cm^2}$ per H atom. This follows from $N(\mathrm{H}) = 5.8\ 10^{21}\ E_{B-V}$ [$\mathrm{cm^{-2}}$] (Bohlin et al. 1978), $\tau_v = N(\mathrm{H})\,\kappa_v$, $A_V/E_{B-V} = 3.1$ and $A_V = 1.086\ \tau_V$. The combined contribution in the FUV of the big particles (Sect. 2.1.1) and the small graphites (Sect. 2.1.2) leaves a residual extinction of the order of κ_V to be explained by the PAHs. Estimates for the FUV cross section of a carbon atom in a PAH range from $5\ 10^{-18}$ to $2\ 10^{-17}\,\mathrm{cm^2}$ (ATB; Omont 1986). If we take the upper limit we find that $\simeq 10\%$ of the total carbon abundance $Y_C = 3\ 10^{-4}$ have to be locked up in PAHs in order to explain the FUV extinction curves. A similar estimate for Y_C^{PAH} follows from the luminosity in the IR features (Léger et al. 1989b). In our model calculations we allow Y_C^{PAH} to vary around the above estimates so that it can be adjusted to the varying photon environment.

2.2.4. Size distribution of PAHs; clusters of PAHs

The temperature of a PAH can be estimated from "line" ratios. The temperature, in turn, is a measure of the heat capacity and thus the size of the PAH (de Muizon et al. 1986, 1988). Very useful bands for this purpose would be the aromatic C−H stretch transitions $v = 1 \rightarrow 0$ at 3.29 μm and $v = 2 \rightarrow 0$ at 1.67 μm. Unfortunately, the latter has not yet been observed. Instead one uses the ratio between the transitions at 3.3, 3.4 and 11.3 μm. From the 3.3/11.3 ratio ATB find large ($\geqq 40$ C atoms), from the 3.3/3.4 ratio small sizes ($\leqq 40$ C atoms). We adopt small PAHs of $N_C^{PAH} = 25$ carbon atoms.

Besides the small PAHs there exist clusters of PAHs. They consist of more than 100 atoms that can produce many modes and they are therefore able to explain the quasi-continuum observed in the wavelength regions from 3.2 to 3.6 μm, 6 to 8 μm and $\lambda > 12$ μm. We assume that in a particular source all clusters have the same number of atoms. The specific value, however, may vary among sources somewhere between 50 and 500. We adopt values from ATB and Bregman et al. (1989).

2.2.5. Hydrogenation of PAHs

The number of H atoms attached to the peripheral rings in a PAH depends on its history and the environment. H atoms are less strongly bound (4.5 eV) than carbon atoms (7.5 eV) and will therefore tend to be removed in hard and strong radiation fields (Léger et al. 1989b). The degree of hydrogenation will affect the band ratios of the C−H to the C=C vibrations. We use the parameter $\alpha_{H/C}$ to describe in a PAH the number of H atoms relative to the C atoms. ATB argue that in clusters of PAHs dehydrogenation becomes ineffective because of their high density of vibrational modes into which the absorbed photon energy is rapidly dumped. We therefore assume different values of $\alpha_{H/C}$ for small PAHs and clusters, $\alpha_{H/C}$ being greater for the latter. Although in coronene ($C_{24}H_{12}$) $\alpha_{H/C} = 0.5$, values of 0.01 and lower are not excluded for astronomical environments.

2.2.6. Emission coefficients and specific heat of PAHs

The specific heat $c(T)$ of a PAH we derive as the derivative of the enthalpy after Eq. (2.2). Alternative values for the specific heat (e.g. Dwek 1986; Puget & Léger 1989) have very little influence on the emission spectra.

We follow for the emission coefficients of a single PAH the discussion by Léger et al. (1989b). The total emission P in a band at wavelength λ integrated over the solid angle 4π is proportional to the number N_H of H atoms in the PAH in case of the 3.3, 8.6 and 11.3 μm bands, and proportional to the number N_C of carbon atoms in the PAH in the case of the underlying continuum and the 6.2, 7.7 μm bands:

$$P = 4\pi\, B_\lambda(T(t))\ \sigma\ \Delta\lambda\ N \quad (2.5)$$

Here t is the time, $T(t)$ the transient temperature, B_λ the Planck function, N is the number of carbon or hydrogen atoms, respectively, σ and $\Delta\lambda$ are given in Table 1. There are slight differences in the numbers cited by Léger et al. (1989b), d'Hendecourt et al. (1989) and by de Muizon et al. (1990). We simplify the profiles of the IR features by triangles where $\Delta\lambda$ gives the width at the 10% emission level. Small PAHs and clusters are treated formally in Eq. (2.5) in an identical manner, although clusters of PAHs do not become so hot because of their larger heat capacity. They therefore emit preferentially at the longer wavelengths. For modelling the quasi-continuum we use

$$\sigma_\lambda = \frac{A}{\lambda} \exp(-(\lambda_m/\lambda)^2)\ [\mathrm{cm^2}] \quad (2.6)$$

with λ in μm, $\lambda_m = 10$ μm and $A = 3.3\ 10^{-20}$ so that the quasi-continuum emission per PAH at wavelength λ integrated over the solid angle 4π becomes

Table 1. Emission coefficients σ and width $\Delta\lambda$ of PAHs [see Eq. (2.5)] after Leger et al. (1989b)

λ (μm)	3.3	6.2	7.7	8.6	11.3
$\sigma(10^{-21}\,\mathrm{cm}^2)$	$35\,N_H$	$4.1\,N_C$	$2.9\,N_C$	$3.0\,N_H$	$47\,N_H$
$\Delta\lambda$ (μm)	0.04	0.17	0.7	0.4	0.3

$$P_\lambda = 4\pi\, B_\lambda(T(t))\, \sigma_\lambda\, N_C. \tag{2.7}$$

The A/λ dependence of σ_λ in Eq. (2.6) for large wavelengths is estimated from absorption measurements of various PAHs in the lab (Léger et al. 1989b). The exponential factor was introduced by Désert et al. (1990) to give a crude estimate for the quasi-continuum in NGC 2023 at $\lambda < 10\,\mu$m. We neglect a possible temperature dependence of σ_λ (Blanco et al. 1990; Flickinger & Wdowiak 1990) as well as visual fluorescence, which is observed as red emission in reflection nebulae (d'Hendecourt et al. 1986; Chlewicki & Laureijs 1986; Furton & Witt 1990) and due to ionized, instead of neutral PAHs (Allamandola et al. 1987); it may account for 20% of the total IR emission of the PAHs (Guhathakuarta & Tyson 1989).

2.3. *Overview of the model parameters*

The basic parameters of the dust components are size and abundance, and for the PAHs additionally the degree of hydrogenation. Some of them are not varied during the modelling because we believe them to be determined from general considerations. These are the abundance of the big grains and the exponent of their size distribution; the abundance of the small graphites, their upper, and to some extent lower size limit as well as the exponent of their size distribution; the number of atoms in the small PAHs and the clusters. Most of the remaining parameters are already fixed by the extinction curve: the abundance of the PAH clusters and the small graphites and the size of the big grains. The degree of freedom in the fit to the IR observations is thus minimized basically to the hydrogenation parameter of the PAHs and their abundance.

3. Photoemission of dust grains

3.1. *Equilibrium temperature T of dust (big grains)*

In a stationary situation we calculate the grain temperature from the balance between the rate of absorbed and emitted energy:

$$4\pi \int \sigma_\lambda J_\lambda \,\mathrm{d}\lambda = 4\pi \int \sigma_\lambda\, B_\lambda(T)\,\mathrm{d}\lambda \tag{3.1}$$

J_λ is the mean intensity averaged over 4π, $B_\lambda(T)$ denotes the Planck-function and σ_λ the absorption cross section.

3.2. *Quantum heating*

Whereas big grains are treated after Eq. (3.1), small grains ($a < 100$ Å) undergo temperature fluctuations and must be handled differently. If such a grain is heated by one energetic photon and does not absorb a second before it has cooled down one speaks of single-photon absorption. It is important for grains with very small cross sections ($a < 10$ Å). For medium sized particles ($10\,\text{Å} \leqq a < 100$ Å) multi-photon events may dominate, which have a dramatic influence on the emission spectrum. The quantum heating of small particles has been studied by numereous workers (Léger & Puget 1984; Draine & Anderson 1985; Pajot et al. 1986a; Dwek 1986; Désert et al. 1986). We follow the method outlines by Guharthakurta & Draine (1989) and divide the accessible enthalpy states of the grain into ordered bins U_k of width ΔU_k and calculate the probability $P_k(t)$ for finding a grain in the k-th bin. The probability that a grain undergoes per unit time a transition from an initial bin U_i to a final one U_f ($i \neq f$) is described by a transition matrix $A_{f,i}$. The transitions are due to heating and cooling. Heating occurs from any bin i to bin $f > i$ and cooling from i always to $i-1$. Finally, one obtains for the emission

$$\varepsilon_\nu = 4\pi \sum_{f=1}^{N} \sigma_\nu \int_0^\infty B_\nu(T)\, \frac{\mathrm{d}P_f}{\mathrm{d}T}\,\mathrm{d}T. \tag{3.2}$$

The temperature intervals are chosen in such a way that the resulting distribution function $\mathrm{d}P/\mathrm{d}T$ changes smoothly. A check that the grid is well sampled follows from comparison of the absorbed and emitted energy. We use typically 60 enthalpy intervals, whereas Lis & Leung (1991) employed a much finer spacing of $N \simeq 200$ grid points. Increasing N does not necessarily improve the accuracy substantially unless one obtains also a smoother distribution $P_k(T)/\Delta U_k$. Even with small $N(\simeq 30)$, which only roughly approximates the distribution function, one may adequately calculate the resulting emission spectrum.

4. Dust emission from selected sources

For a few sources there exist, besides broad band photometric data, measurements of high spectral resolution ($\lambda/\Delta\lambda \geqq 50$) in the near and mid IR which clearly show the PAH features. We discuss these sources in a sequence of rising strength and harshness of the UV field.

4.1. *The solar neighborhood*

The appropriate extinction curve is that of the diffuse medium (Mathis 1990), and the IR emission refers to high latitude diffuse clouds. Table 2 lists the salient observations. As A_V towards the galactic pole is 0.11 mag the hydrogen column density becomes $N(\mathrm{H}) = 2.1\ 10^{20}\,\mathrm{cm}^{-2}$; all intensities integrated over 4π are given in W/H-atom (Boulanger & Pérault 1988). The 900 μm measurement of $5\ 10^{-8}\,\mathrm{W\,m^{-2}\,ster^{-1}}$ by Pajot et al. (1986b, 1989) towards the galactic center region with an assumed $A_V = 50$ mag has been transformed in Table 2 to the emission from the galactic pole by multiplying it with $4\pi\ 0.11/50\,N(\mathrm{H})$.

The interstellar radiation field is tabulated by Pérault et al. (1988). Our fit to the overall IR spectrum is encouraging (Fig. 1a), but due to the paucity of mid IR observations it is not unique. Figure 1b illustrates how the different dust components contribute to the various sections of the extinction curve. Model

Table 2. IR observations in the solar neighborhood

λ (μm)	$\Delta\lambda$ (μm)	U_ν (W/H-atom)	Reference
3.3	0.05	$2.5 \pm 1.30\ 10^{-31}$	Giard et al. (1988)
12	5.7	$1.1 \pm 0.30\ 10^{-31}$	Boulanger & Pérault (1988)
25	9.8	$0.7 \pm 0.20\ 10^{-31}$	Boulanger & Pérault (1988)
60	31	$1.1 \pm 0.06\ 10^{-31}$	Boulanger & Pérault (1988)
100	35.6	$3.2 \pm 0.12\ 10^{-31}$	Boulanger & Pérault (1988)
102	30.6	$2.5 \pm 0.50\ 10^{-31}$	Lange et al. (1989)
137	48	$3.9 \pm 0.80\ 10^{-31}$	Lange et al. (1989)
262	94	$7.2 \pm 3.60\ 10^{-32}$	Lange et al. (1989)
325	250	$7.1 \pm 2.10\ 10^{-32}$	Fabbri et al. (1986)
900	296	$6.5(\cdot 2^{\pm 1})\ 10^{-34}$	Pajot et al. (1989)

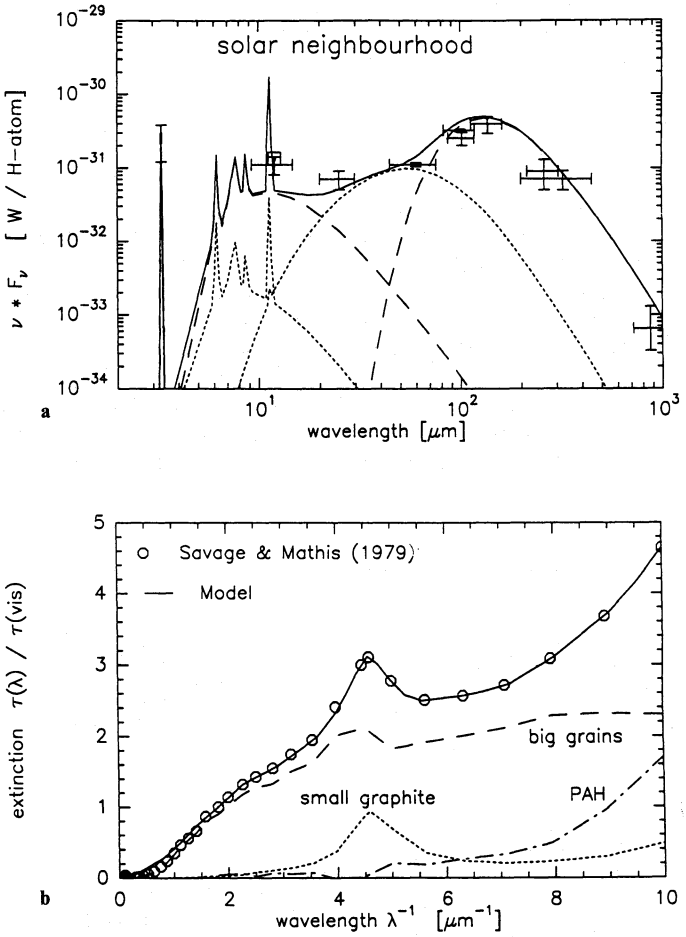

Fig. 1a and b. Dust model of the solar neighborhood. **a** Emission spectrum, observations (crosses) are listed in Table 2, the model is given by the full line. The square at 12 μm is also a model result and was calculated by convolving the full line with the IRAS transmission curve. **b** Mean interstellar extinction curve, circles are data after Savage & Mathis (1979), full line refers to our model. In both figures we show the contribution of the three dust components separately: *big grains* (dashed) are responsible for the linear rise in the extinction curve and for emission in the FIR and submm region; *small graphites* (dotted) explain the 2175 Å bump and the mid IR shoulder; *PAHs*, both small ones and clusters, are needed for the non-linear rise in the FUV (das-dotted), and the near and mit IR emission. In particular, the continuum at $\lambda \leqq 20\,\mu$m is due to PAH clusters (dashed) and the 3.3 μm feature is due to small PAHs (dotted). Note that the small grains emit $\simeq$40% of the total IR energy

parameters are listed in Table 3. The strong 3.3 μm feature is interpreted by small PAHs, and not by the PAH clusters which are on the average too cold. The other resonances have not yet been measured. We achieve excellent agreement with the 12 μm IRAS observation. The broad emission plateau from 60 down to, at least, 10 μm cannot be explained by big grains and is due to small particles. PAH clusters also contribute to the 25 μm emission. The small graphite grains account for the 25 and 60 μm flux and the large grains are only responsible for the emission $\lambda \geqq 100\,\mu$m. Therefore, the IRAS ratio S_{60}/S_{100} refers to fluxes from two different dust components and does not measure a physical grain temperature. PAHs and small graphites emit 40% of the total luminosity.

4.2. The reflection nebula N 2023

The nebula, located at a distance $D = 500$ pc, is associated with the molecular cloud L1630 (Milman et al. 1975; Morris et al. 1974), a C II and a compact H II region (Knapp et al. 1975; Pankonin & Walmsley 1976). Its size is estimated from photographic plates to $\simeq 6'$ ($2\,r_0 = 0.9$ pc). Data on the illuminating star HD 37903 are given by Lee (1968), Racine (1968) and references therein. It is of type B1.5 V, implying a luminosity $L_* = 9.9\ 10^3\,L_\odot$ and an effective temperature $T_* = 21\,500 \pm 1000$ K, and suffers a reddening $E_{B-V} = 0.36$ mag corresponding to an extinction $A_V = 1.1$ mag assuming $R = 3.1$. However, from a recent NIR study by DePoy et al. (1990) a much smaller obscuration seems more likely and is also supported by our model.

The extinction curve towards HD 37903 after Fitzpatrick & Massa (1988), see Fig. 2 and Table 3, is not very different from the standard curve, but has a less pronounced bump and lower FUV extinction. Therefore the abundance of the graphites per H-atom is only $Y_C = 4\ 10^{-5}$. The emission of the nebula shows the PAH features in the IR as well as an underlying flat continuum between 1 to 13 μm from hot dust with a black body temperature of 1000 K (Sellgren et al. 1985). Its color temperature does not change out to a few tenths of pc from the exciting star (Sellgren et al. 1990a).

The luminosity in the IRAS bands equals $1100\,L_\odot$ and is thus much less than the stellar luminosity. Harvey et al. (1980) find a luminosity from 40 to 350 μm of $1900\,L_\odot$. Both results imply that most of stellar radiation escapes without being absorbed by dust. Altogether, the nebula is very clumpy and extinction changes rapidly on small scales (Gatley et al. 1987; DePoy et al. 1990). Because of the low extinction towards HD 37903 we need not

Table 3. Parameters of dust components in various environments. The abundance Y denotes the fraction of carbon atoms locked up in grains relative to H in the interstellar medium. The following parameters, not shown in the Table, are kept constant: volume in cm^3 per H-atom of amorphous carbon ($2.1\ 10^{-27}$) and silicate ($3.1\ 10^{-27}$); exponent of the size distribution for big grains (silicate and amorphous carbon) $q = 3.5$ and for small graphite grains $q = 4$; upper size limit of small graphites $a_+^{gr} = 75$ Å; number of carbon atoms in small PAHs $N_C^{PAH} = 25$

Object		Local Sun	N 2023	N 7023	N 7027	Orion POS 4
Model parameter	Notation					
Amorphous carbon						
Lower size	a_-^{ac} (Å)	300	300	300	300	600
Upper size	a_+^{ac} (Å)	1200	1200	1200	600	2400
Silicate						
Lower size	a_-^{si} (Å)	150	300	300	300	1200
Upper size	a_+^{si} (Å)	1800	2400	2400	1200	9600
Small graphite						
Lower size	a_-^{gr} (Å)	4.7	4.7	4.7	4.7	9.3
Abundance	Y_c^{gr} (10^{-5})	5.0	4.0	5.0	5.0	0.5
Central wavelength of the bump	λ_c (Å)	2175	2167	2175	2175	2157
FWHM	γ (μm^{-1})	0.992	1.045	0.992	0.992	0.846
Small PAH						
Abundance	Y_c^{PAH} (10^{-5})	2.4	0.061	1.3	0.24	0.21
H/C atom ratio	$\alpha_{H/C}^{PAH}$	0.4	0.05	0.1	0.03	0.02
PAH cluster						
Abundance	Y_c^{clu} (10^{-5})	3.0	0.28	4.48	1.49	0.28
H/C atom ratio	$\alpha_{H/C}^{clu}$	0.5	0.2	0.15	0.15	0.2
Number of C atoms	N_c^{clu}	150	140	64	298	400

consider the detailed radiative transfer. The location of HD 37903 along the line of sight is not established, but the star cannot be too close to the nebula as otherwise one would observe big grains at high temperatures. The star is also not at the centroid of FIR map (Harvey et al. 1980). We assume that the dust emission originates at a distance $r \simeq 0.3$ pc $\simeq 9\ 10^{17}$ cm.

The color temperature of the source between 60 and 1300 μm is 20 to 25 K. Modelling the FIR emission of the big grains for distances $r = 9\ 10^{17}$ cm leads to dust temperatures which are at least a factor of two higher. This discrepancy can be explained in three ways: (a) The emission at $\lambda > 60$ μm comes from an additional component of cold dust located in the neighboring molecular cloud. This is the explanation we favor because the molecular cloud behind N 2023 observed in CO (Gatley et al. 1987) must make some contribution to the FIR emission. The source for this FIR luminosity may be either HD 37903 itself or some of the other young and highly obscured stars in this region. We therefore assume an additional component of cold dust of $90\ M_\odot$ and $T_d = 20$ K. (b) The reflection nebula is further away from the star than $9\ 10^{17}$ cm. Although we can then fit the FIR data, the mass of the big as well as the small grains becomes too large and, consequently, we overestimate the 12 and 25 μm flux. A further reduction of the abundance of the small grains causes problems in fitting the extinction curve. (c) The spectrum of the flux impinging on the reflection nebula is no longer that of a B 1.5 star, but has been softened by dust absorption and reemission between HD 37903 and N 2023. However, such extinction of stellar light disagrees with the result of DePoy et al. (1990).

In the reflection nebula the grains at distance r are illuminated by a flux F_λ:

$$F_\lambda = \frac{L_*}{4 r^2 \sigma T_*^4} B_\lambda(T_*) \exp(-\tau_\lambda). \quad (4.1)$$

We evaluate their emission for the distance $r = 9\ 10^{17}$ cm and $\tau_V \simeq 0.1$ appropriate for the locus where the measurements have been made and assume that this position is typical for the whole nebula. The amorphous carbon grains of 300 (1200) Å radius then attain an equilibrium temperature of 65 (50) K; the silicate grains of 300 (2400) Å acquire 55 (41) K. The total mass of interstellar matter required to explain the optically thin emission is $\simeq 0.5\ M_\odot$. Assuming a constant density distribution one finds a mean visual optical depth to the cloud of $A_V \simeq 0.04$ mag. At 12 and 25 μm the flux of the model depends sensitively on the abundance and size distribution of the graphite particles and the PAH cluster. PAH parameters follow from an analysis of the near IR spectrum. It was observed only 60″ south of HD 37903, but is assumed to be representative for the whole nebula. A fit to the dust emission and the extinction curve is depicted in Fig. 2.

The 1 to 14 μm spectrum taken 60″ S of HD 37903 is shown in Fig. 3. The data have been read off Fig. 1 in Sellgren et al. (1985) together with the error bars. Our model for this position has a column density through the cloud of $N_H = 2.2\ 10^{21}\ cm^{-2}$ corresponding to $A_V = 1.1$ mag, which is much larger than the mean extinction. The model values have been convolved with the resolution of the spectrometer ($\lambda/\Delta\lambda = 100$). Beside the feature at 8.6 μm, which is underestimated by a factor of 3, the continuum emission at 5.6 and in the 9–11 μm region is not fit perfectly. However, taking all uncertainties about PAHs into account (UV absorption cross sections, emission coefficients, abundance and size, deactivation rate by IR fluorescence), the model is quite

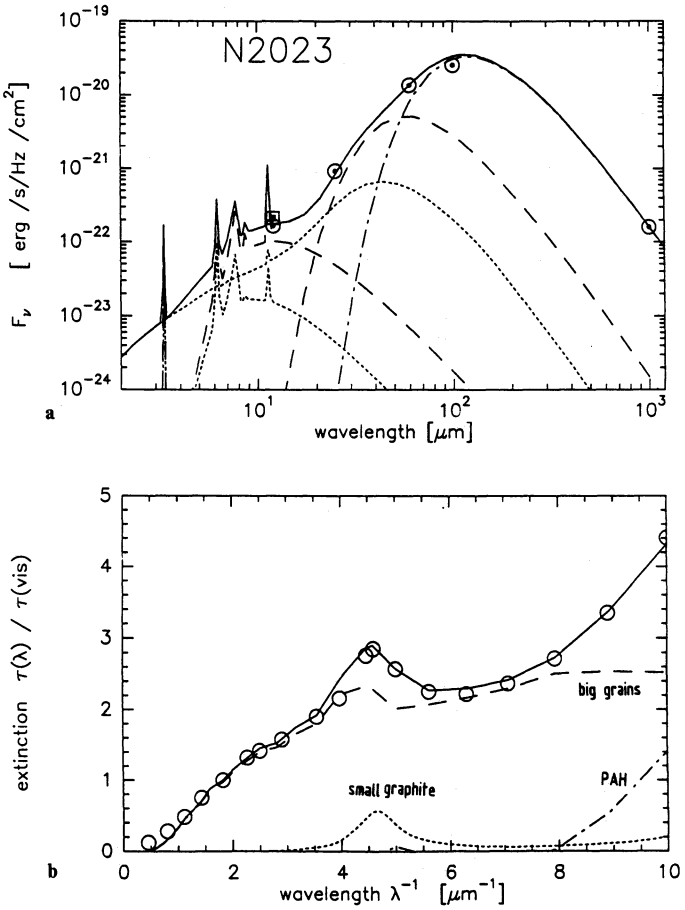

Fig. 2. **a** Broad band spectrum of the entire reflection nebula N 2023. IRAS fluxes and 1.3 mm point (Chini et al. 1984) are shown by circles, the model by a solid line. The square at 12 μm is calculated by convolving the full line with the IRAS transmission curve. As explained in the text, the emission at $\lambda \geqq 100$ μm is ascribed to cold dust in the background cloud L 1630 (dash-dotted). The dust components are from left to right: small PAHs (dotted), PAH clusters (dashed), small graphites (dotted), big grains (dashed). **b** Extinction curve towards HD 37903. Full line is again our model, circles are observational data. Individual dust components are shown separately. "PAH" refers to the joint contribution from small PAHs and clusters.

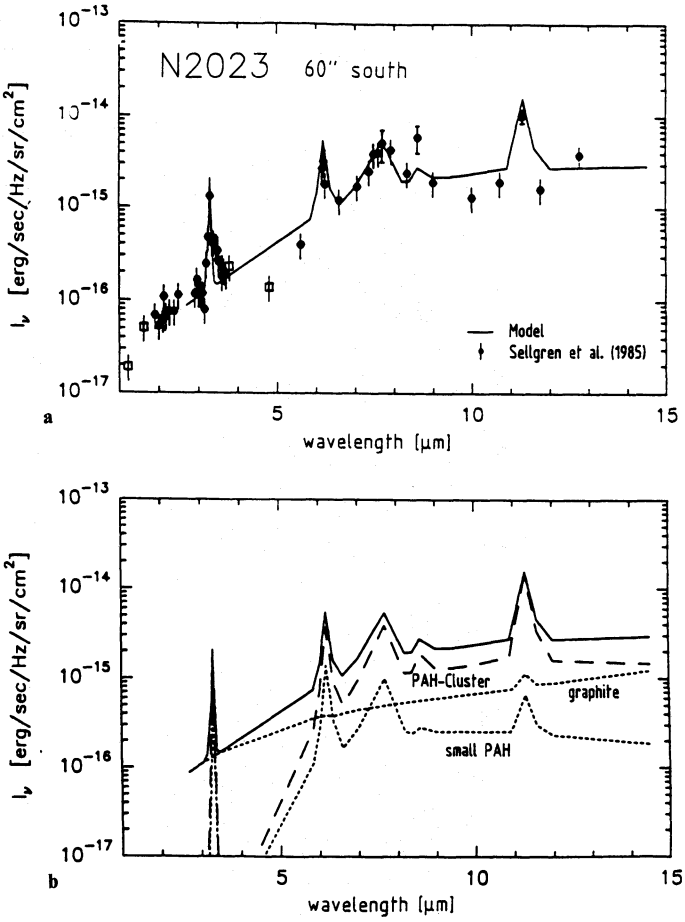

Fig. 3. **a** 3 to 14 μm spectrum of N 2023 taken 60″ S of the exciting star after Sellgren et al. (1985). Broad band observations are marked by squares. But for the 8.6 μm feature, the model is within the uncertainties of the measurements. **b** Full line is our model. We show separately the emission of the small PAHs, which are responsible for the 3.3 μm feature, the PAH clusters and the graphites. Big grains are negligible at these wavelengths

successful. The contributions of the dust components between 3–12 μm clearly show (Fig. 3b) that the 3.3 μm feature is due to the small PAHs, the continuum between 3–7 μm to small graphites and the continuum at longer wavelength ($\lambda \leqq 14$ μm) to PAH clusters. Big grains are much too cold to contribute.

4.3. The reflection nebula N 7023

The nebula lies at a distance of $D = 440$ pc (Viotti 1969) in the northern part of a huge (30′ × 60′) dark cloud. Its size is estimated from photographic plates to $\simeq 4'$ ($2r = 0.5$ pc). It is illuminated by HD 200775 classified as B3IVe with $T_* = 17000$ K (Strom 1972), $L_* = 4000\, L_\odot$ and $E_{B-V} = 0.48$ mag or $A_V = 1.5$ mag (Racine 1968; Whitcomb et al. 1981). N 7023 shows thin filamentary structures up to 6′ from the exciting star and knots in the inner part of the cloud (2′ × 3′) (Witt & Cottrell 1980). Submm and FIR observations of N 7023 are summarized in Table 3 of Whitcomb et al. (1981). Spectrophotometric data ($\Delta\lambda/\lambda = 100$) and broad band measurements between 2 to 14 μm taken 30″ W and 20″ N of HD 200775 are given in Sellgren et al. (1985).

The emission spectrum is calculated in the same manner as for N 2023. In Eq. (4.1) we adopt $r = 0.13$ pc $\simeq 4\ 10^{17}$ cm and $\tau_V = 1.2$, the exact values are not crucial. We assume towards HD 200775 the mean interstellar extinction curve. For amorphous carbon and small graphite grains we use dust parameters as in the solar neighborhood, but somewhat bigger silicates to fit the submm data (Table 3). Our fits to the extinction curve and the broad band measurements are very satisfactory (Fig. 4). The total mass of interstellar matter required to explain the IR emission is 3.1 $M_\odot$; for comparison, an $A_V = 1.5$ mag leads for a homogeneous sphere of $r = 0.25$ pc radius to $\simeq 9\, M_\odot$. The small graphites account for the 25 μm IRAS band and the big particles for the emission at $\lambda \geqq 50$ μm. The big carbon grains of 300 (1200) Å radius attain a temperature of 43 (38) K; the silicates of 300 (2400) Å reach 34 (30) K.

The 12 μm model point (square in Fig. 4a) is helpful to confine the parameters of the PAHs. The PAH clusters are responsible for

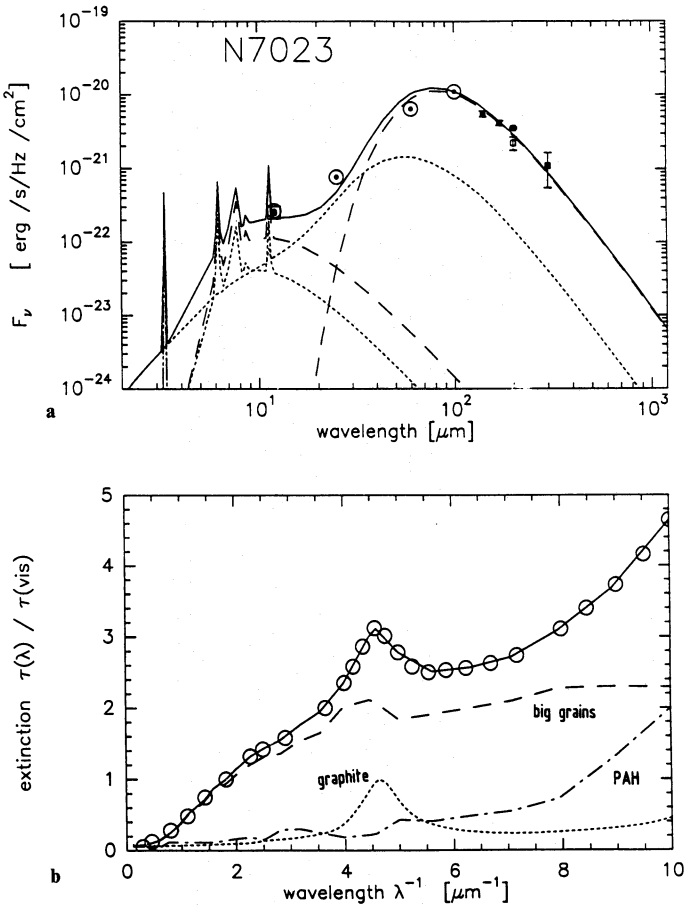

Fig. 4. **a** Broad band spectrum of the entire reflection nebula N 7023. IRAS fluxes are shown by circles, all other FIR/submm points are after Whitcomb et al. (1981). The model is depicted by a solid line. The square at 12 μm, which almost coincides with the IRAS point, is calculated by convolving the full line with the IRAS transmission curve. The dust components are from left to right: small PAHs (dotted), PAH clusters (dashed), small graphites (dotted), big grains (dashed). **b** We assume towards N 7023 the extinction curve of the solar neighborhood, see Fig. 2b

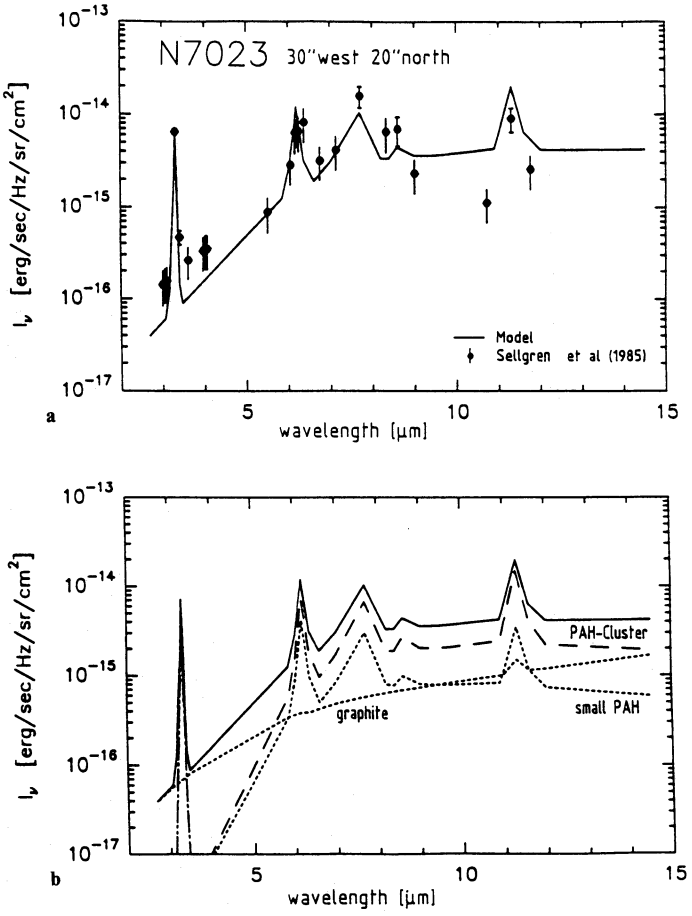

Fig. 5. **a** 3 to 14 μm spectrum of N 7023 taken 30″ W and 20″ N of the exciting star after Sellgren et al. (1985). **b** See Fig. 3b

the 12 μm emission as they are cooler than the small PAHs. Using a cluster size for N 7023 after ATB we are left with only two free parameters: the cluster abundance Y_C^{clu} and the degree of hydrogenation $\alpha_{H/C}^{clu}$. The first of these is restricted by the FUV extinction and the latter by the 3 to 13 μm high resolution spectrum (Fig. 5). It was taken 30″ W and 20″ N of HD 200775; we assume that the properties of the PAHs at this position are representative for the nebula.

The 3.3 μm feature is also well reproduced; the weaker 3.4 μm resonance was not modeled and the 8.6 μm feature, barely seen in the observations, is weakly indicated in the model. The fits to the remaining PAH features at 6.2, 7.7, 11.3 μm are quite reasonable. The discrepancy between observation and theory between 9 to 11 μm reflects the uncertainties in the estimates of the quasi-continuum (Eq. 2.6), which are in this wavelength region due to the PAH clusters (Fig. 5b). The overall fit to the extinction curve, to the broad band and, where available, the spectrophotometric measurements is encouraging. Note that the stellar emission for HD 200775 is in the 1 to 4 μm region on a 5 to 10 Jy level (Fig. 9 in Sellgren 1984).

4.4. *The planetary nebula N 7027*

The nebula is at a distance of $D = 880 \pm 150$ pc (Masson 1989). The luminosity ($L_* = 8400\, L_\odot$) and effective temperature ($T_* = 3.7\ 10^5$ K) of the central star are from Fig. 6 in Pottasch (1982). The exciting radiation field is modeled after Eq. (4.1) with $r = 2\ 10^{16}$ cm and $\tau_V = 0.1$. We use for the reddening towards N 7027 the standard extinction curve; at least, it is an excellent approximation between $6563\,\text{Å} \geqq \lambda \geqq 1640\,\text{Å}$ (Seaton 1979). Therefore the sizes for the big grains and the small graphites are the same as in the solar neighborhood.

We present a good fit to the the total IR spectrum (Fig. 6a). The emission at 1.3 mm (Chini et al. 1984) is due to bremsstrahlung, and not to dust, as it can be directly extrapolated by $\nu^{-0.1}$ from the cm radio region.

N 7027 is carbon-rich ([C]/[O] ≃ 3.5, Shields 1978) and therefore PAHs are expected to be abundant (Cohen et al. 1986). One observes a broad plateau from 10.5 to 12.5 μm (Aitken & Roche 1983) as well as strong PAH features between 3 and 12 μm. A study from 16 to 23 μm with $\Delta\lambda = 0.5$ μm (dots in Fig. 6a) and from 20 to 38 μm with $\Delta\lambda = 1.2$ μm (circles) did not reveal additional broad resonances (McCarthy et al. 1978). Shure et al. (1983) found several gaseous lines. To explain the mid IR emission one does not need small graphites because the big grains are already sufficiently hot. The spectrum between 3 and 14 μm (Fig. 7) shows many features, including gas emission lines as well as dust resonances.

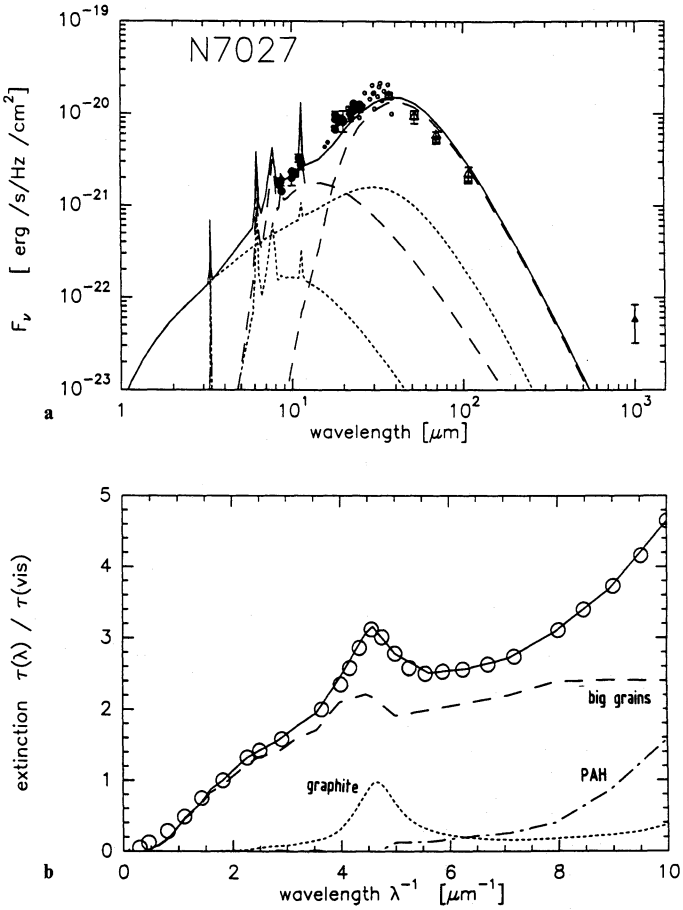

Fig. 6. **a** Total spectrum of the planetary nebula N 7027 containing observations of high resolution (small filled and open circles) and broad band measurements (all other symbols). Observations are from Gillett et al. (1973), Becklin et al. (1973), Jameson et al. (1974), Dyck & Simon (1976), Telesco & Harper (1977) and Bentley (1982, see his Table 1). Full line refers to our model. The dust components are from left to right: small PAHs (dotted), PAH clusters (dashed), small graphites (dotted), big grains (dashed). References in the text. **b** See Fig. 4b

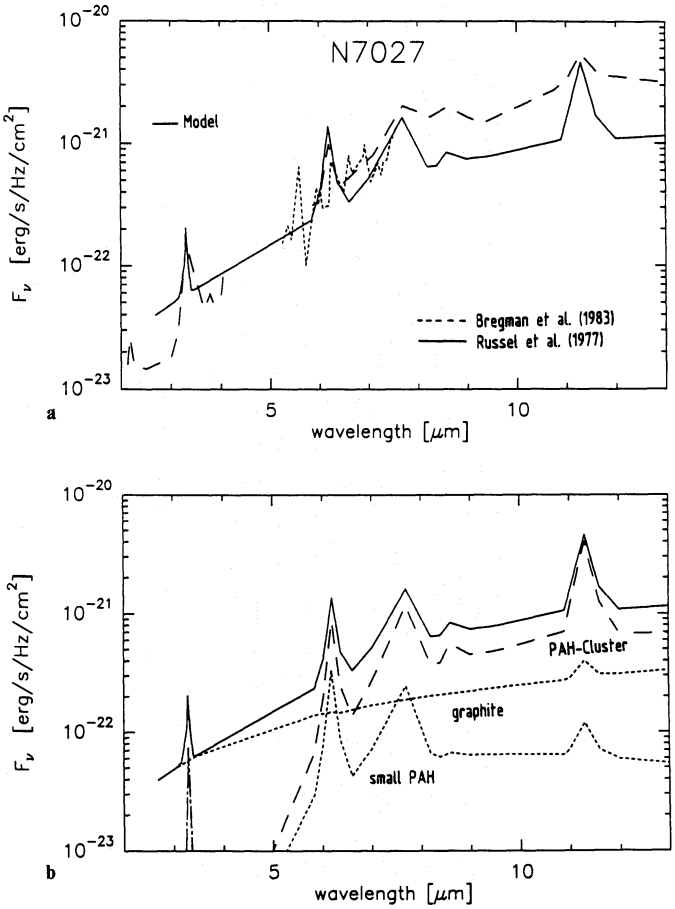

Fig. 7. **a** 3 to 14 μm spectrum of N 7027. The high resolution data, which are very numerous, are from Fig. 2 in Russell et al. (1977) (2 μm$\leqq\lambda\leqq$14 μm with $\lambda/\Delta\lambda$=65) and Fig. 1 in Bregman et al. (1983) (5.2 μm$\leqq\lambda\leqq$7.5 μm with $\lambda/\Delta\lambda$=120–200). Those data have been read off graphically and are approximated here by a dashed and a dotted line, respectively. The solid line refers to our model. **b** See Fig. 3b

The 3.3 μm feature has been studied with very high spectral resolution: from $\Delta\lambda/\lambda = 400$ by Geballe et al. (1985) who detected the 3.4 μm resonance and an emission plateau centered at 3.45 μm up to $\Delta\lambda/\lambda = 4000$ by Lowe et al. (1991) who resolved some of the broad resonances into individual components; they rule out PAHs greater than coronene for the 3 μm region. In our model highly dehydrogenated small PAHs are responsible for the 3.3 μm feature (Fig. 7b). The continuum for $\lambda < 6$ μm is due to small graphites and the spectrum from 6 to 20 μm to PAH clusters (Fig. 6a, 7b). The model, calculated for a resolution of $\Delta\lambda/\lambda = 65$, can explain all dust features and the continuum within a factor of 2. It is also in agreement to better than 30% with the broad band measurements of Bentley (1982) (not shown in Fig. 6a).

Goebel et al. (1987) observed the 8 to 14 μm region and concluded that the C=C and C−H bands are excited in different regions of the nebula. The spatial distribution of the mid IR features is discussed by Aitken & Roche (1983). A comparison of the distribution of the 3.3 μm feature with Brα lines at 4.052 μm shows (Woodward et al. 1987) that (a) PAHs are also excited in non-ionized regions and peak strongly just outside the ionized gas; (b) a high rate of Lyman photons leads to PAH destruction. This spatial distribution is further discussed for the Orion bar.

4.5. The Orion bar

4.5.1. Overall description

In the Orion nebula (D=460 pc) the interface between the H II region and the neutral gas SE of the Trapezium is called the bar. It is viewed edge-on and prominently seen in the mid IR. Aitken et al. (1979) obtained spectra from 8 to 13 μm at several positions in the nebula; they detected the 12.8 μm Ne II line and concluded that PAHs ("unidentified features") dominate the mid IR. Sellgren (1981) mapped a large part of the nebula in the resonance at 3.3 μm and in the continuum at 3.5 μm and found for them quite different intensity distributions. The 3.3 μm feature peaks at the interface between ionized and neutral gas between the maxima of the Brackett lines and the molecular H_2 gas (Sellgren et al. 1990b; Hayashi et al. 1985). Geballe et al. (1989) found in high resolution spectra at 3 μm that some of the weaker features vary spatially independently of each other. Roche et al. (1989) detect in 11 to 13 μm spectra over a region 10″ N to 20″ S of the peak, referenced henceforth as position 4, fine structure in the 11.3 μm resonance, (possibly solo C−H bend at 11.05 μm) and a broad feature at 12.7 μm (possibly three peripheral H atoms in edge carbon rings,

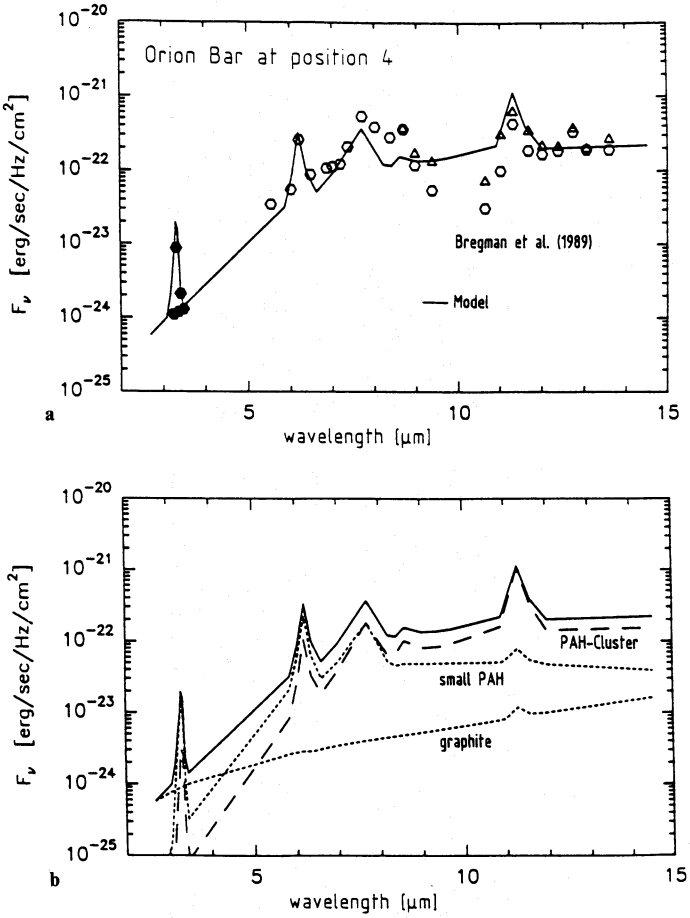

Fig. 8. **a** 3 to 14 μm spectrum of the ionisation front in Orion at position 4. The model is given by the solid line. Data are read off Fig. 1 in Bregman et al. (1989): (*filled circles*: 3 μm region with 5″ aperture from UKIRT; *open circles*: 5 to 8 μm region with 21″ aperture from KAO and 8 to 12.8 μm region with 6″ aperture from 1.5 m Mount Lemmon telescope; *triangles*: 8.6 to 13 μm region with 3″ aperture from IRTF normalized to the Mount Lemmon data). **b** See Fig. 3b

see Sect. 2.2.1). A normalized spectrum of the whole range between 3 to 14 μm towards position 4 is published by Bregman et al. (1989).

4.5.2. The 3 to 14 μm spectrum towards position 4

The exciting radiation field there is modeled after Eq. (4.1) using values with respect to θ^2 Ori A: $\tau_v = 1$ (Werner 1982), $L_* = 50\,000\,L_\odot$, $T_* = 25\,000$ K and $r = 3.2\ 10^{17}$ cm; the trapezium stars are neglected because of their larger distance ($8\ 10^{17}$ cm). We adopt the extinction curve towards θ^2 Ori C (Fitzpatrick & Massa 1988) assuming that it does not vary across the nebular region. Because of its large A_V/E_{B-V} ratio, weak bump and very flat shape in the FUV small graphites and PAHs must be underabundant and amorphous grains be larger than in the solar neighborhood (Table 3). Size estimates of the small PAHs after ATB, Geballe et al. (1989) and Bregman et al. (1989) confirm our model value of $N_C^{PAH} = 25$ carbon atoms per small PAH; for the PAH clusters we follow Bregman et al. (1989) and use $N_C^{clu} = 400$. This leaves only the hydrogenation parameters $\alpha_{H/C}^{PAH}$, $\alpha_{H/C}^{clu}$ to be adjusted to the high resolution spectrum.

In our model the big grains do not contribute to the 3 to 14 μm region because their temperatures are too low: for carbon grains with 600 (2400) Å radius $T = 85$ (50) K and for silicate particles with 1200 (9600) Å radius $T = 64$ (45) K. The depression in the spectrum between 9 to 11 μm is not the silicate feature as the optical depth is too low; it may be just a trough between the resonances at 8.6 and 11.3 μm. According to Fig. 1 of Bregman et al. (1989) the continuum itself, after subtraction of the emission in the resonances, shows a minimum around 10 μm, but the reality of this continuum is controversial. In any case, as our model gives only a crude approximation to the quasi-continuum emission of PAHs (Eq. 2.6) we do not aim at reproducing such details.

Very small graphite particles become unstable in strong and harsh UV environments. Adopting a minimum size $a_-^{gr} = 9.3$ Å, instead of $a_-^{gr} = 4.7$ Å derived from the sublimation rate, leads to a better match of the $\lambda < 5$ μm continuum. The 12.8 μm Ne II line and the 12.7 μm broad feature seen by Roche et al. (1989) are neglected in our model. The 8.6 μm feature is not well reproduced, but it is weak and superposed on the shoulder of the broad resonances in the 8 μm region. The 3.3, 6.2, 7.7 and 11.3 μm features are fit successfully. Keeping in mind that also laboratory studies of PAHs do not give a perfect match to astronomical spectra our overall fit is satisfactory.

4.5.3. The variation of the 5 to 8 μm spectra across the Bar

The spatial distribution in the 5 to 8 μm region was determined by Bregman et al. (1989) at position 4, 10″ north and 10″ and 20″ south of it. We assume for the exciting radiation field the same parameters as for position 4, but modify the projected distance, i.e. from north to south $r = 3.1$, 3.2 (position 4), 3.4 and 3.8, respectively, in units of 10^{17} cm. The UV field at position 4 ($\tau_{UV} \simeq 2$) is over seven times stronger than 20″ south of it. This is consistent with the estimates of Geballe et al. (1989), who use the 3.29 μm feature as a direct measure for the UV flux. At all positions we keep the size of the PAHs constant, the total amount of atoms (C plus H) in clusters is 500. (For instance, at position 4: $N_C^{clu} = 400$ and $\alpha_{H/C}^{clu} = 0.2$, see Table 4). Our model fits the spatial distribution for $\lambda \geqq 5.5$ μm within the uncertainties. PAHs are important for the 6.2 μm features, but the 7.7 μm resonance is dominated by the clusters. Note that the small graphites (dotted) do not affect the spectrum.

In hostile UV environments (north of position 4) the PAHs are less abundant and less hydrogenated compared to weaker radiation fields. The hydrogenation parameter of the small PAHs (PAH clusters) therefore decreases from 10% (30%) 20″ S of position 4 to 1% (10%) 10″ N of it. From our modeling a scenario emerges for the photo-fragmentation of PAHs (see also Fig. 8 of Schutte et al. 1990): (i) Far away from the UV source the small PAHs and the clusters are hydrogenated. (ii) Closer to the star first the small PAHs and then the clusters lose their H-atoms because the clusters have more vibrating modes over which they can distribute the photon energy; (iii) Below a critical distance all PAHs have lost all hydrogen atoms; (iv) In the stellar vicinity the harsh UV environment destroys even the PAH skeletons.

5. Conclusions

We model simultaneously the extinction and emission in four classes of objects with progressively increasing UV flux. The emphasis is placed on the interpretation of the IR features and continuum radiation from PAHs and small graphite particles. By this effort we obtain a dust model that is in agreement with the presently available data. It has the following components:

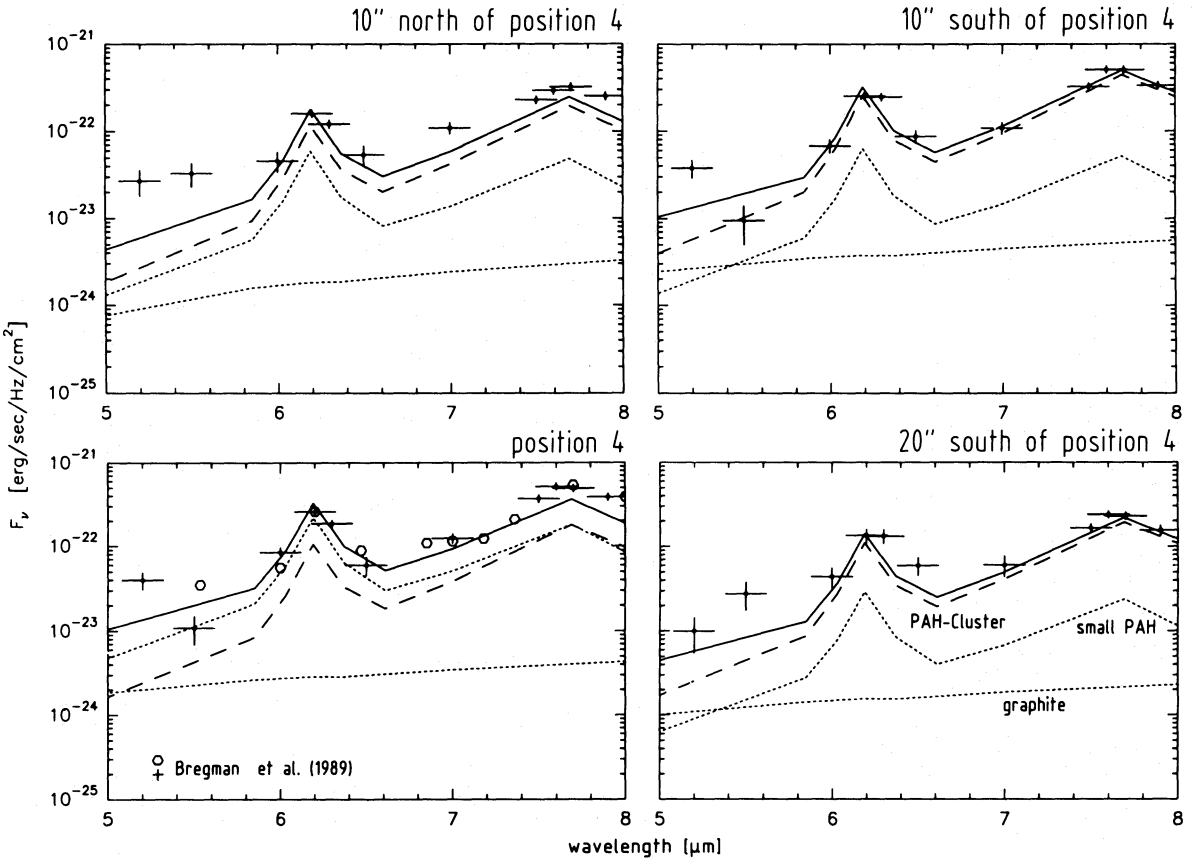

Fig. 9. Spatial distribution of the dust emission in the Orion Bar: 5 to 8 μm spectra taken in the Orion bar at position 4, 10″N, 10″S and 20″S of it. Full line is model. Circles are from Fig. 1 and crosses from Fig. 2 of Bregman et al. (1989)

Table 4. Photochemical distribution of PAHs across the Orion Bar

Parameter		10″N	Pos. 4	10″S	20″S
Distance, $r(10^{17}\,\mathrm{cm})$		3.1	3.2	3.4	3.8
Small PAHs (total: 25 atoms)					
H/C atom ratio	$\alpha_{H/C}^{PAH}$	0.01	0.02	0.1	0.1
Abundance	Y_C^{PAH}	$2.5\ 10^{-7}$	$1.0\ 10^{-6}$	$1.1\ 10^{-6}$	$1.4\ 10^{-6}$
PAH clusters (total: 500 atoms)					
H/C atom ratio	$\alpha_{H/C}^{clus}$	0.1	0.2	0.3	0.3
Abundance	Y_C^{clus}	$2.7\ 10^{-6}$	$2.8\ 10^{-6}$	$2.5\ 10^{-5}$	$2.8\ 10^{-5}$

(a) The classical large grains ($a > 100$ Å) of astronomical silicate and amorphous carbon produce the far IR emission and the extinction for $\lambda > 2500$ Å. Their properties are described by the MRN model. They do not vary much among the sources considered here, except that their sizes are generally larger in Orion, but this is well understood in the framework of the MRN model in terms of a large A_V/E_{B-V} ratio. As the temperature of the classical grains digresses only slightly from an equilibrium value it is straight forward to calculate their emission provided one knows the optical constants of the grain material. We have not considered here that the grains are probably fluffy and have a very complex structure.

(b) Small particles of graphitic carbon ($a \leqq 75$ Å) are necessary not only to explain the 2175 Å extinction bump, for which they were first introduced, but also to account for the mid IR emission. They have to be small in order to explain the constancy of the central wavelength of the 2175 Å resonance and, consequently, undergo temperatures fluctuations. We incorporate this effect, including multi-photon heating, when calculating their time averaged emission. Their spectrum peaks at 30 to 50 μm and often dominates over the large particles at $\lambda \leqq 30$ μm. In the solar neighborhood, where the large grains are cool ($\simeq 20$ K) they account even for the 60 μm emission. The minimum radius a_-^{gr} of small graphites, which lies typically at 5 Å, is determined by evaporation. This is in line with our model of Orion where a_-^{gr} changes from 5 to 10 Å as one approaches the exciting star. As small graphites probably have a steeper than normal size distribution with an exponent $q = 4$, their mass is contained in the

smallest particles. Their abundance ratio by mass over the large carbon grains is around 1:5, except for Orion, where it has dropped to 1:50. This can qualitatively be explained by the evaporation of the smallest grains.

(c) PAHs are best identified by their characteristic near and mid IR bands. They also show a continuum, although quantitatively less determined, which dominates the spectrum of our sources for $5 < \lambda < 14\,\mu m$. Emission of PAHs is activated only in an environment of energetic photons ($> 7\,eV$). Because they consist of a small number of atoms their excitation state fluctuates strongly and a thermal treatment, except at high temperatures, is dubious. PAHs are thought to occur in two forms: as isolated molecules and in clusters. Both are much more variable in size, abundance and structure than the large grains. This behavior they have in common with molecules which are also much more susceptible to the conditions of the environment, especially the radiation field. The models for our sources and for the positions within Orion yield different structures of the PAHs. We ascribe these changes to variations in the strength and hardness of the radiation field. In particular, we find that in a sequence of declining harshness of the radiation field, from the solar neighborhood over reflection nebulae to H II regions or planetaries, the degree of hydrogenation $\alpha_{H/C}$ decreases. It also decreases in the case of fixed harshness (Orion bar) as one comes closer to the exciting star. We derive a similar drop as for $\alpha_{H/C}$ for the abundance of the PAHs, both for single molecules and clusters. PAHs are also a good candidate for explaining the non-linear extinction rise in the far UV.

To confirm our hypothesis of the photochemical evolution of the PAHs a *normalized* 3 to 14 μm spectrum, as it is available for position 4, is necessary for each of the other three positions. Such observations should be carried out with spectral resolution $\Delta\lambda/\lambda \simeq 100$ in order to resolve the strong PAH features and with diaphragms of $\simeq 5''$ to avoid spatial overlap.

References

Aitken D.K., Roche P.F., Spenser P.M., Jones B., 1979, A&A 76, 60
Aitken D.K., Roche P.F., 1983, MNRAS 202, 1233
Allamandola L.J., Tielens A.G.G.M., Barker J.R., 1985, ApJ 290, L25
Allamandola L.J., Tielens A.G.G.M., 1987, Interstellar Processes, Hollenbach D.J., Thronson H.A. (eds.), Reidel, Dordrecht, p. 471
Allamandola L., Tielens A., Barker J., 1989, ApJS 71, 733 (ATB)
Allamandola L., et al., 1990, ApJ 345, L59
Barker J., Cherchneff I., 1989, IAU Symp. 135, 197
Becklin E.E., Neugebauer G., Wynn-Willams C.G., 1973, ApJ 15, 87
Bentley A.F., 1982, ApJ 87, 1810
Blanco A., Fonti S., Orofino L., 1990, ApJ 364, 152
Bohlin R.C., Savage B.D., Drake J.F., 1978, ApJ 224, 132
Boulanger F., Perault F., 1988, ApJ 330, 964
Bregman J.D., et al., 1983, ApJ 274, 666
Bregman J.D., Allamandola L.J., Tielens A., Geballe T.R., Witteborn F.C., 1989, ApJ 344, 791
Bussoletti E., Fusco C., Longo G., 1988, Experiments on Cosmic Dust Analogoues, Kluwer, Dordrecht
Cardelli J.A., Clayton G.C., Mathis J.S., 1989, ApJ 345, 245
Chase M.W., Davies C.A., Downey J.R., Frurip D.J., McDonald R.A., Syverud A.N., 1985, J. Phys. Chem. Ref. Data 14, Suppl. No. 1
Chlewicki G., Laureijs R.J., 1986, Polycyclic Aromatic Hydrocarbons, Leger A., et al. (eds.), p. 335
Chini R., Kreysa E., Mezger P.G., Gemünd H.-P., 1984, A&A 137, 117
Cohen M., Allamandola L., Tielens A., Bregman J., Simpson J.P., Witteborn F.C., Wooden D., Rank D., 1986, ApJ 302, 737
de Muizon M.J., Geballe T., d'Hendecourt L., Baas F., 1986, ApJ 306, L105
de Muizon M.J., d'Hendecourt L.B., Geballe T.R., 1988, Infrared Spectroscopy in Astronomy, Proceeding of the 22nd ESLAB Symposium in Salamanca, p. 177
de Muizon M.J., d'Hendecourt L.B., Geballe T.R., 1990, A&A 227, 526
DePoy D.L., Lada A., Gatley I., Probst R., 1990, ApJ 356, L55
Desert F.-X., Boulanger F., Shore S.N., 1986, A&A 160, 295
Desert F.-X., Boulanger F., Puget J.L., 1990, A&A 237, 215
d'Hendecourt L.B., Leger A., Olofsson G., Schmidt W., 1986, A&A 170, 91
d'Hendecourt L.B., et al., 1989, IAU Symp. 135, 207
Draine B.T., Anderson N., 1985, ApJ 292, 494
Draine B.T., 1985, ApJS 57, 587
Draine B.T., 1988, ApJ 333, 848
Draine B.T., 1989, IAU Symp. 135, 313
Dwek E., 1986, ApJ 302, 363
Dyck H.M., Simon T., 1976, PASP 88, 738
Edoh O., 1983, Ph.D thesis, University of Arizona
Fabbri R., et al., 1986, proceed. of Marcel Grossman Meeting, Rome, June 1985, p. 985
Fitzpatrick E.L., Massa D., 1988, ApJ 328, 734
Flickinger G.C., Wdowiak T.J., 1990, ApJ 362, L71
Furton D.G., Witt A.N., 1990, ApJ 364, L45
Gatley I., Hasegawa T., Suzuki H., Garden R., Brand P., Lightfoot J., Glencross W., Okuda H., Nagata T., 1987, ApJ 318, L73
Geballe T.R., et al., 1985, ApJ 292, 500
Geballe T.T., Tielens A., Allamandola L.J., Moorhouse A., Brand P.W.J.L., 1989, ApJ 341, 278
Giard M., et al., 1988, A&A 201, 278
Gillett F.C., Forrest W.J., Merrill K.M., 1973, ApJ 183, 87
Goebel J.H., Rank D., Cohen M., 1987, Infrared Astronomy with Arrays, Wynn-Williams C.G., Becklin E.E. (eds.), p. 299
Guhathakurta P., Draine B.T., 1989, ApJ 345, 230
Guhathakurta P., Tyson J.A., 1989, IAU Symp. 139, 210
Harvey P.M., Harley A.T. Jr., Gatley I., 1980, ApJ 235,, 894
Hayashi M., Hasegawa T., Gatley I., Garden R., Kaifu N., 1985, MNRAS 215, 31
Huffman D., 1989, IAU Symp. 135, 329
IRAS Explanatory Supplement, 1985, Beichman C., et al. (eds.)
Jameson R.F., et al., 1974, ApJ 190, 353
Knapp G.R., Brown R.L., Kuiper T.B.H., 1975, ApJ 196, 167
Lange A.E., et al., 1989, IAU Symp. 135, p. 499
Lee T.A., 1968, ApJ 152, 913
Leger A., Puget J.L., 1984, A&A 137, L5
Leger A., Verstraete L., d'Hendecourt L., Defourneau D., Dutuit D., Schmidt W., Lauer J., 1989a, IAU Symp. 135, 173
Leger A., d'Hendecourt L., Defourneau D., 1989b, A&A 216, 148
Lis D.C., Leung C.M., 1991, ApJ 372, L107
Lowe R.P., Moorhead M., Wehlau W.H., Maillard J.-P., 1991, ApJ 368, 195
Masson C.R., 1989, ApJ 336, 294
Mathis J.S., Rumpl W., Nordsieck K.H., 1977, ApJ 217, 425

Mathis J.S., Whiffen G., 1989, ApJ 341, 808
Mathis J.S., 1990, ARA&A 28, 37
McCarthy J.F., Forrest W.J., Houck J.R., 1978, ApJ 224, 109
Milman A.S., Knapp G.R., Kerr F.J., Knapp S.L., Wilson W.J., 1975, ApJ 80, 93
Morris M., Palmer P., Turner B.E., Zuckerman B., 1974, ApJ 191, 349
Nuth J.A., 1987, Ap. Space Sic. 139, 103
Omont A., 1986, A&A 164, 159
Pajot F., Boisse P., Gispert R., Lamarre J.M., Puget J.L., Serra G., 1986a, A&A 157, 393
Pajot F., et al., 1986b, A&A 154, 55
Pajot F., et al., 1989, A&A 223, 107
Pankonin V., Walmsley C.M., 1976, A&A 48, 341
Perault M., Boulanger F., Puget J.L., Falgarone E., 1988, ApJ (submitted)
Pottasch S.R., 1982, IAU Symp. 102, p. 391
Puget J.L., Leger A., 1989, ARA&A 27, 161
Racine R., 1968, AJ 73, 233
Robin M.B., 1974, Higher Excited States of Polyatomic Molecules, Vol. 2. New York Academic
Roche P.F., Aitken D.K., Craig H.S., 1989, MNRAS 236, 485
Russell R.W., Soifer B.T., Willner S.P., 1977, ApJ 217, L149
Schutte W.A., Tielens A., Allamandola L., Cohen M., Wooden D.H., 1990, ApJ 360, 577
Seaton M.J., 1979, MNRAS 187, 785
Sellgren K., 1981, ApJ 245, 138
Sellgren K., 1984, ApJ 277, 623
Sellgren K., Allamandola L., Bregman J.D., Werner M.W., Wooden D.H., 1985, ApJ 299, 416
Sellgren K., Luan L., Werner M.W., 1990a, ApJ 349, 120
Sellgren K., Tokunaga A.T., Nakada Y., 1990b, ApJ 349, 120
Shields G.A., 1978, ApJ 219, 565
Shure M.A.T., Herter J.R., Houck J.R., Briotta D.A. Jr., Forrest W.J., Gull G.E., McCarthy J.F., 1983, ApJ 270, 645
Sorrell W.H., 1989, MNRAS 214, 89
Sorrell W.H., 1990, MNRAS 243, 570
Strom S.E., 1972, ApJ 173, 353
Telesco C.M., Harper D.A., 1980, ApJ 235, 392
Viotti R., 1969, Mem. Soc. Astron. Ital. 40, 75
Werner M.W., 1982, Symposium on the Orion Nebula, Glassgold et al. (eds.), p. 32
Whitcomb S.E., Gatley I., Hildebrand R.H., Keene J., Sellgren K., Werner M.W., 1981, ApJ 246, 416
Witt A.N., Cottrell M.J., 1980, AJ 85, 22
Woodward C.E., Pipher J.L., Shure M.A., Forrest W.J., Sellgren K., Nagata T., 1987, Infrared Astronomy with Arrays, Wynn-Williams G., Becklin E. (eds.), p. 299